arXiv:astro-ph/0210598v1 28 Oct 2002

# Stellar Populations and Star Cluster Formation in Interacting Galaxies with the Advanced Camera for Surveys [1]

Richard de Grijs [a,2], Jessica T. Lee [b], M. Clemencia Mora Herrera [c], Uta Fritze–v. Alvensleben [d], and Peter Anders [d]

[a] *Institute of Astronomy, University of Cambridge, Madingley Road, Cambridge CB3 0HA, UK*

[b] *Department of Astronomy, Harvard University, 60 Garden Street, Cambridge, MA 02138, USA*

[c] *Departamento de Astronomía y Astrofísica, Facultad de Física, Pontifícia Universidad Católica de Chile, V. Vicuña Mackenna 4860 Macul, Santiago, Chile*

[d] *Universitätssternwarte, University of Göttingen, Geismarlandstr. 11, 37083 Göttingen, Germany*

**Abstract**

Pixel-by-pixel colour-magnitude and colour-colour diagrams – based on a subset of the *Hubble Space Telescope* Advanced Camera for Surveys Early Release Observations – provide a powerful technique to explore and deduce the star and star cluster formation histories of the Mice and the Tadpole interacting galaxies.

In each interacting system we find some 40 bright young star clusters ($20 \lesssim$ F606W(mag) $\lesssim 25$, with a characteristic mass of $\sim 3 \times 10^6 M_\odot$), which are spatially coincident with blue regions of active star formation in their tidal tails and spiral arms. We estimate that the main events triggering the formation of these clusters occurred $\sim (1.5 - 2.0) \times 10^8$ yr ago. We show that star cluster formation is a major mode of star formation in galaxy interactions, with $\gtrsim 35\%$ of the active star formation in encounters occurring in star clusters. This is the first time that young star clusters have been detected along the tidal tails in interacting galaxies.

The tidal tail of the Tadpole system is dominated by blue star forming regions, which occupy some 60% of the total area covered by the tail and contribute $\sim 70\%$ of the total flux in the F475W filter (decreasing to $\sim 40\%$ in F814W). The remaining pixels in the tail have colours consistent with those of the main disk. The tidally triggered burst of star formation in the Mice is of similar strength in both interacting galaxies, but it has affected only relatively small, spatially coherent areas.

*Key words:* galaxies: evolution, galaxies: individual: NGC 4676, UGC 10214, galaxies: interactions, galaxies: star clusters, galaxies: stellar content

*PACS:* 98.20.Jp, 98.62.Ai, 98.62.Lv

## 1 Introduction

Integrated broad-band colours have been used extensively to study the global star formation histories (SFHs) of elliptical and spiral galaxies and of spiral bulges. However, integrated colours are almost always dominated by the light from the central regions of the galaxies or by bulge light.

The use of resolved multi-passband colour data has only recently been pioneered in efforts to disentangle *local* stellar populations from dust and extinction effects in the disks and bulges of nearby spiral galaxies (e.g. Balcells & Peletier 1994, Terndrup et al. 1994, de Jong 1996, Peletier & Balcells 1996, Peletier et al. 1999, Eskridge et al. 2002) and in intermediate-redshift galaxies in the Hubble Deep Field (Franceschini et al. 1998, Abraham et al. 1999). Probably the most detailed studies of spatially resolved stellar populations to date are the recent analysis of M81 by Kong et al. (2000), and Eskridge et al. (2002)'s ultraviolet–optical colour analysis of *Hubble Space Telescope (HST)* images of NGC 6753 and NGC 6782. The use of resolved galaxy colours, i.e., the colours of spatially resolved areas of galactic disks, allows the study of localised extinction, age distributions and SFHs of spatially distinct components within a given galaxy, with highly robust results (e.g. Bothun 1986, de Jong 1996, Abraham et al. 1999, Peletier et al. 1999, Eskridge et al. 2002).

### *1.1 The Single Stellar Population approximation*

The distribution of colours and spectral energy distributions (SEDs) across the face of a given galaxy is the cumulative result of the way in which the local stellar population has been assembled, and of projection effects.

In this paper we will, as a first-order approximation, assume that the in-

[1] Based on archival observations with the NASA/ESA *Hubble Space Telescope*, obtained at the Space Telescope Science Institute, which is operated by the Association of Universities for Research in Astronomy (AURA), Inc., under NASA contract NAS 5-26555.

[2] Corresponding author.
*E-mail addresses:* grijs@ast.cam.ac.uk (RdeG), lee45@fas.harvard.edu (JTL), mcmora@puc.cl (MCMH), ufritze@uni-sw.gwdg.de (UFvA), panders@uni-sw.gwdg.de (PA)

tegrated *local* colours throughout our galaxy images are sufficiently closely represented by either a single or a superposition of multiple single stellar populations (SSPs; Kong et al. 2000), i.e. a single generation of coeval stars with fixed parameters such as metallicity, initial mass function (IMF), and internal extinction (see Buzzoni 1997). This will allow us to analyse the properties and SFH of the stellar population *that dominates the light* at a given wavelength. We note that while this approximation holds relatively well for young, luminous stellar populations, at older ages the underlying galactic population is not well represented anymore by a *single* stellar population. However, as we will show below, for older ages ($t \gtrsim 10^9$ yr) the age vectors of the individual SSPs in colour-colour space (defined by the passbands used in this paper) are almost parallel to each other, so that any deviation from the SSP approximation will only have a very small effect.

The use of the relatively well-understood SSPs for the interpretation of localised colours instead of more complex SFHs simplifies our interpretation, while the adoption of more complex SFHs changes neither the results nor the interpretation *qualitatively* (see e.g. Kong et al. 2000).

In this paper we follow the recent pioneering studies by Abraham et al. (1999) and Eskridge et al. (2002) in constructing colour-colour and colour-magnitude diagrams (CC, CMDs) on a pixel-by-pixel basis. This technique was first used by Bothun (1986), who used a $B$ vs. $(B-R)$ CMD to analyse the stellar populations in NGC 4449. While Abraham et al. (1999) employed the technique to intermediate-redshift galaxies, in Eskridge et al. (2002) we brought it back to the study of stellar populations in the local Universe. Here, we explore for the first time the advantages of using this type of pixel mapping technique in interacting galaxies. Galaxy interactions induce violently star-forming episodes, which are expected to leave signatures in the victims' CC diagrams and CMDs in the form of distinct features that can be traced back to, for instance, newly formed stellar populations and their associated dust lanes.

Although the local Universe contains a mere handful of interacting systems at various stages of their gravitational embrace, the addition of the high-resolution Advanced Camera for Surveys (ACS) to the *HST* suite of instruments has increased the applicability of pixel-mapping techniques to interacting systems at greater distances. Since the ACS is somewhat undersampled by its point-spread function (PSF) at optical wavelengths, the individual pixels are statistically independent.

In Section 2, we give a brief overview of the archival *HST* images used for our analysis, and of the data reduction process. We will then present our results in Section 3, which we interpret in the context of star and star cluster formation induced by the gravitational interactions in Section 4. For a brief summary of the main results and conclusions, we refer the reader to Section 5.

## 2 ACS observations and reduction: the Tadpole and Mice galaxies

Our analysis of the star clusters in and SFHs of the interacting galaxies UGC 10214 (Arp 188; VV 029; the "Tadpole" galaxy) and NGC 4676 (Arp 242; VV 224; first nicknamed "The [Playing] Mice" galaxies by Vorontsov-Vel'yaminov (1958)) is based on the Early Release Observations (EROs) obtained with the ACS onboard *HST*. The field of view (FOV) of these images, taken as part of programme GO-8992 (PI Ford), was adjusted to optimise the sampling of the tidal tails and debris surrounding both systems.

Broad-band images through the F475W, F606W and F814W filters (roughly corresponding to Johnson-Cousins broad-band *B, V* and *I* filters, respectively) of both systems were obtained with the ACS/Wide Field Camera (WFC), the instrument of choice for red-optimised optical observations with the *HST*. The ACS/WFC consists of two parallel rectangular $2048 \times 4096$ thinned, back-illuminated Scientific Imaging Technologies (SITe) CCDs, separated by a $\sim 2''$ gap. With a pixel size of $\sim 0\farcs05$, the total FOV is $202'' \times 202''$; this set-up provides a good compromise between adequately sampling the PSF and a wide FOV (e.g. Pavlovsky et al. 2001). For both fields, the observations were taken with a relative vertical offset of $\sim 3''$ to be able to fill in the gap between the two WFC chips. The ACCUM imaging mode was used to preserve dynamic range and to facilitate the removal of cosmic rays.

The observations of the Mice were taken on 7 April 2002 (UT); those of the Tadpole galaxy were obtained on 1 and 9 April 2002 (UT). The total exposure times of the observations of the Mice used in this paper are 4650s, 4150s, and 3450s in F475W, F606W and F814W, respectively. The corresponding total exposure times for the Tadpole images are 13780s, 7610s and 8360s.

We used the (CALACS) pipeline-processed data products provided by the *HST* archive, which include the recalibration with new flat fields (dated 6 August 2002). These are expected to result in a generic large-scale photometric uniformity level of the images of $\sim 1\%$. In particular, for our analysis we used the final, dithered images produced by the most recent release of the *PyDrizzle* software tool. *PyDrizzle* also performs a geometric correction on all ACS data, using fourth-order geometric distortion polynomials, and subsequently combines multiple images into a single output image and converts the data to units of count rate at the same time.

We registered the individual images obtained for all passbands and for both galaxy systems to high (subpixel) accuracy, and created combined images for each galaxy/passband combination, using the appropriate IMALIGN and IMCOMBINE routines in IRAF/STSDAS [3].

[3] The Image Reduction and Analysis Facility (IRAF) is distributed by the National

## 3 The distribution of ages, colours and dust

### *3.1 The brightest star clusters*

With the unprecedented combination of resolution and field of view offered by the ACS, it has now become possible to resolve and study (at least the bright end of) the star cluster luminosity function (CLF) out to greater distances than ever before. In this section, we give the full observational details for the clusters in the bright wing of the CLFs of both of our targeted systems.

The ongoing tidal interactions between both galaxies of the Mice, and the tidal disruption of a smaller satellite galaxy by the dominant Sc-type spiral galaxy in the Tadpole system have caused highly variable galactic backgrounds in both systems. In addition, the high sensitivity of the ACS, combined with the long exposure times used for these EROs, reveals large numbers of background galaxies in the frames of both interacting systems. Both of these aspects render the unambiguous detection of genuine star cluster candidates troublesome.

We based our initial selection of source candidates on a modified version of the DAOFIND task in the DAOPHOT software package (Stetson 1987), running under IDL, in which we selected all potential sources with peak luminosities – in any of the passbands – brighter than $5\sigma_{\rm sky}$, i.e. five times the noise in the sky background (see Section 3.2). We required our star cluster candidates to meet the following stringent selection criteria:

- Good star cluster candidates must be detected in all of the F475W, F606W, and F814W passbands. Upper limits in any of the passbands make a direct comparison with the underlying galactic stellar populations impossible, or highly uncertain at best.
- Their sizes must be of the same order as the ACS PSF, i.e., $\sigma_{\rm cl} \geq \sigma_{\rm PSF}$. Ground-based test measurements and artificial PSFs generated by TinyTim (Krist & Hook 2001) show that the ACS PSF is $\sim 0.8 - 1.0$ pixels. The onboard performance is affected by optical aberrations and geometric distortions. Point sources imaged with the WFC also experience blurring due to charge diffusion into adjacent pixels because of CCD subpixel variations (e.g. Pavlovsky et al. 2001). We adopted a conservative size selection criterion of $\sigma_{\rm cl} \gtrsim 0.8$ pixel.

Optical Astronomy Observatories, which is operated by the Association of Universities for Research in Astronomy, Inc., under cooperative agreement with the National Science Foundation. STSDAS, the Space Telescope Science Data Analysis System, contains tasks complementary to the existing IRAF tasks. We used Version 2.3 (June 2001) for the data reduction performed in this paper.

- Genuine star clusters should not be significantly elongated, so that we limited the roundness parameter in DAOFIND to fall in the range $[-1.0, 1.0]$.
- Finally, the candidate clusters must be associated with the galaxies, but we do not want to exclude objects that may have been ejected from the main body of the system due to gravitational kicks. Therefore, we required their (conservative) maximum projected distance to be $2\farcs0$ and $1\farcs5$ from the $3\sigma_{\rm sky}$ contours of the Mice and the Tadpole galaxies, respectively. At their respective distances (distance moduli $m - M = 34.93$ and 35.70, based on their Virgocentric radial velocities and $H_0 = 70$ km s$^{-1}$ Mpc$^{-1}$), this corresponds to a maximum projected distance of $\sim 1$ kpc in both cases.

Finally, we visually verified all of the star cluster candidates by simultaneously displaying enlargements of them in all three passbands, and assigned appropriate annuli for aperture photometry to obtain source and sky background fluxes. Our final cluster samples contain 45 and 38 sources for the Mice and the Tadpole, respectively. We used standard aperture radii for the source fluxes of 20 ACS pixels ($\sim 1\farcs01$), and determined the sky background in annular rings with radii $20 \leq r \leq 32$ pixels ($1\farcs01 \lesssim r \lesssim 1\farcs61$), although in a few individual cases these annuli had to be adjusted to include all of the source flux or avoid bright features in the background annuli. Photometric calibration to the STMAG system was achieved by applying the image header keywords PHOTFLAM and PHOTZPT to the total count rates for each cluster. As photometric zero-point offsets we used 25.564, 26.538 and 26.706 for F475W, F606W and F814W, respectively. Our bright cluster samples are characterised by brightnesses of $20 \lesssim$ F606W(mag) $\lesssim 25$ in both systems. A proper completeness analysis is severely complicated by the highly variable extinction and (galactic) background levels across the individual interacting galaxies, and by the small sizes of our objects.

In Tables 1 and 2 we list the clusters' coordinates, properly corrected for the geometric distortions inherent to the optical design of the ACS, and their photometric properties in all passbands. The photometric uncertainties include the effects of Poisson-type noise, and variations and shot noise in the background annuli. Due to the almost parallel age and extinction vectors, we cannot correct our magnitude measurements for the effects of extinction (but see Section 4). This clearly shows, therefore, that the particular combination of F475W, F606W and F814W passbands by itself is not a good choice for age estimates based on broad-band colours, for objects older than $\sim 10^8$ yr.

### *3.2 Properties of the interacting systems as a whole*

The analysis of broad-band galaxy colours in terms of their SFHs and stellar content is complicated due to the composite nature of the galaxy's stellar

Table 1
Characteristics of the brightest star clusters in the Mice

| No. | R.A. (J2000) (hh mm ss.ss) | Dec (J2000) (dd mm ss.ss) | F475W (ST mag) | F606W (ST mag) | F814W (ST mag) |
|---|---|---|---|---|---|
| 1 | 12 46 10.35 | 30 45 28.44 | $23.446 \pm 0.064$ | $23.342 \pm 0.026$ | $24.074 \pm 0.037$ |
| 2 | 10.34 | 27.65 | $22.968 \pm 0.033$ | $23.069 \pm 0.022$ | $24.127 \pm 0.040$ |
| 3 | 10.33 | 22.47 | $22.619 \pm 0.029$ | $22.826 \pm 0.023$ | $23.430 \pm 0.027$ |
| 4 | 10.81 | 23.64 | $25.647 \pm 0.181$ | $26.014 \pm 0.173$ | $26.087 \pm 0.159$ |
| 5 | 10.36 | 12.39 | $21.677 \pm 0.021$ | $22.098 \pm 0.020$ | $22.798 \pm 0.025$ |
| 6 | 10.30 | 44 49.12 | $20.658 \pm 0.015$ | $21.196 \pm 0.018$ | $21.794 \pm 0.019$ |
| 7 | 10.86 | 50.57 | $24.819 \pm 0.101$ | $24.717 \pm 0.075$ | $24.653 \pm 0.063$ |
| 8 | 10.29 | 31.03 | $20.338 \pm 0.015$ | $20.733 \pm 0.016$ | $21.348 \pm 0.018$ |
| 9 | 10.19 | 30.32 | $20.779 \pm 0.038$ | $21.141 \pm 0.039$ | $21.707 \pm 0.040$ |
| 10 | 10.31 | 30.59 | $20.695 \pm 0.016$ | $21.063 \pm 0.015$ | $21.657 \pm 0.015$ |
| 11 | 10.28 | 28.49 | $20.665 \pm 0.019$ | $21.165 \pm 0.021$ | $21.858 \pm 0.023$ |
| 12 | 10.30 | 28.46 | $20.732 \pm 0.020$ | $21.198 \pm 0.021$ | $21.900 \pm 0.024$ |
| 13 | 10.29 | 27.70 | $20.782 \pm 0.020$ | $21.274 \pm 0.021$ | $21.978 \pm 0.025$ |
| 14 | 10.19 | 22.20 | $23.397 \pm 0.294$ | $23.690 \pm 0.276$ | $24.291 \pm 0.301$ |
| 15 | 10.22 | 21.35 | $21.325 \pm 0.033$ | $21.938 \pm 0.041$ | $22.385 \pm 0.039$ |
| 16 | 10.28 | 17.25 | $21.772 \pm 0.048$ | $22.155 \pm 0.047$ | $22.696 \pm 0.048$ |
| 17 | 10.22 | 16.68 | $21.270 \pm 0.022$ | $21.780 \pm 0.025$ | $22.448 \pm 0.030$ |
| 18 | 10.28 | 17.31 | $21.737 \pm 0.046$ | $22.117 \pm 0.044$ | $22.673 \pm 0.046$ |
| 19 | 10.18 | 09.86 | $21.622 \pm 0.031$ | $22.084 \pm 0.031$ | $22.842 \pm 0.037$ |
| 20 | 10.44 | 07.33 | $23.620 \pm 0.077$ | $24.192 \pm 0.120$ | $24.501 \pm 0.141$ |
| 21 | 09.96 | 43 59.67 | $20.266 \pm 0.049$ | $20.689 \pm 0.059$ | $21.239 \pm 0.072$ |
| 22 | 09.67 | 57.67 | $21.940 \pm 0.067$ | $21.826 \pm 0.063$ | $21.933 \pm 0.064$ |
| 23 | 09.92 | 58.44 | $19.372 \pm 0.024$ | $19.735 \pm 0.027$ | $20.323 \pm 0.033$ |
| 24 | 10.00 | 51.50 | $20.154 \pm 0.027$ | $20.301 \pm 0.044$ | $19.353 \pm 0.023$ |
| 25 | 09.50 | 43.01 | $23.123 \pm 0.077$ | $22.861 \pm 0.072$ | $22.944 \pm 0.080$ |
| 26 | 09.98 | 44.36 | $19.678 \pm 0.014$ | $19.770 \pm 0.014$ | $20.595 \pm 0.023$ |
| 27 | 09.75 | 26.74 | $23.879 \pm 0.082$ | $23.492 \pm 0.037$ | $23.840 \pm 0.040$ |
| 28 | 09.97 | 25.09 | $24.255 \pm 0.095$ | $24.875 \pm 0.125$ | $25.557 \pm 0.197$ |
| 29 | 11.79 | 34.79 | $21.428 \pm 0.038$ | $21.848 \pm 0.042$ | $22.753 \pm 0.062$ |
| 30 | 11.35 | 31.69 | $22.523 \pm 0.052$ | $23.050 \pm 0.075$ | $24.033 \pm 0.132$ |
| 31 | 11.40 | 30.11 | $21.798 \pm 0.022$ | $21.884 \pm 0.022$ | $22.692 \pm 0.050$ |
| 32 | 09.59 | 16.66 | $23.547 \pm 0.038$ | $22.950 \pm 0.015$ | $22.107 \pm 0.006$ |
| 33 | 12.22 | 27.03 | $23.832 \pm 0.216$ | $24.255 \pm 0.238$ | $24.508 \pm 0.202$ |
| 34 | 12.20 | 24.18 | $22.821 \pm 0.043$ | $23.201 \pm 0.044$ | $23.806 \pm 0.050$ |
| 35 | 12.16 | 21.43 | $23.261 \pm 0.038$ | $23.576 \pm 0.040$ | $24.319 \pm 0.068$ |
| 36 | 11.99 | 19.37 | $21.962 \pm 0.041$ | $22.262 \pm 0.045$ | $22.963 \pm 0.067$ |
| 37 | 12.44 | 16.80 | $22.741 \pm 0.033$ | $22.822 \pm 0.028$ | $22.917 \pm 0.023$ |
| 38 | 11.58 | 03.80 | $23.756 \pm 0.049$ | $24.331 \pm 0.047$ | $24.797 \pm 0.060$ |
| 39 | 10.73 | 42 55.36 | $24.886 \pm 0.110$ | $24.981 \pm 0.070$ | $25.735 \pm 0.121$ |
| 40 | 12.00 | 43 02.46 | $22.512 \pm 0.017$ | $23.076 \pm 0.019$ | $23.787 \pm 0.027$ |
| 41 | 12.75 | 03.20 | $24.860 \pm 0.100$ | $24.244 \pm 0.031$ | $24.098 \pm 0.022$ |
| 42 | 11.77 | 42 56.56 | $24.073 \pm 0.063$ | $24.397 \pm 0.051$ | $25.212 \pm 0.082$ |
| 43 | 11.25 | 49.30 | $25.123 \pm 0.137$ | $25.497 \pm 0.106$ | $25.625 \pm 0.099$ |
| 44 | 11.58 | 49.95 | $23.949 \pm 0.051$ | $24.464 \pm 0.046$ | $25.107 \pm 0.066$ |
| 45 | 12.12 | 47.39 | $25.303 \pm 0.144$ | $25.504 \pm 0.091$ | $25.126 \pm 0.059$ |

Table 2
Characteristics of the brightest star clusters in the Tadpole

| No. | R.A. (J2000) (hh mm ss.ss) | Dec (J2000) (dd mm ss.ss) | F475W (ST mag) | F606W (ST mag) | F814W (ST mag) |
|---|---|---|---|---|---|
| 1 | 16 06 24.54 | 55 26 06.37 | $24.442 \pm 0.017$ | $24.795 \pm 0.034$ | $25.487 \pm 0.020$ |
| 2 | 23.47 | 07.44 | $25.804 \pm 0.104$ | $25.307 \pm 0.084$ | $26.223 \pm 0.082$ |
| 3 | 21.64 | 14.45 | $24.464 \pm 0.017$ | $24.593 \pm 0.029$ | $25.653 \pm 0.024$ |
| 4 | 22.93 | 03.13 | $25.415 \pm 0.047$ | $25.361 \pm 0.057$ | $26.294 \pm 0.053$ |
| 5 | 22.58 | 25 56.79 | $24.521 \pm 0.024$ | $24.829 \pm 0.047$ | $26.003 \pm 0.043$ |
| 6 | 19.83 | 57.53 | $21.116 \pm 0.015$ | $21.721 \pm 0.017$ | $22.585 \pm 0.021$ |
| 7 | 15.79 | 50.85 | $21.407 \pm 0.006$ | $21.894 \pm 0.008$ | $23.079 \pm 0.010$ |
| 8 | 15.77 | 50.93 | $21.393 \pm 0.006$ | $21.894 \pm 0.008$ | $23.074 \pm 0.010$ |
| 9 | 15.06 | 44.18 | $23.008 \pm 0.010$ | $23.955 \pm 0.029$ | $24.091 \pm 0.013$ |
| 0 | 08.08 | 29.69 | $24.824 \pm 0.078$ | $23.804 \pm 0.029$ | $22.816 \pm 0.007$ |
| 11 | 06.96 | 32.37 | $24.932 \pm 0.417$ | $24.704 \pm 0.324$ | $25.748 \pm 0.650$ |
| 12 | 06.64 | 32.65 | $21.541 \pm 0.022$ | $21.702 \pm 0.023$ | $21.978 \pm 0.022$ |
| 13 | 05.56 | 35.12 | $22.134 \pm 0.055$ | $22.431 \pm 0.063$ | $22.774 \pm 0.059$ |
| 14 | 03.57 | 45.37 | $24.977 \pm 0.183$ | $24.540 \pm 0.104$ | $24.563 \pm 0.051$ |
| 15 | 07.33 | 19.84 | $25.279 \pm 0.056$ | $24.937 \pm 0.053$ | $26.185 \pm 0.062$ |
| 16 | 06.01 | 28.49 | $21.384 \pm 0.036$ | $21.726 \pm 0.041$ | $22.522 \pm 0.059$ |
| 17 | 05.47 | 30.49 | $21.651 \pm 0.044$ | $21.796 \pm 0.051$ | $22.722 \pm 0.095$ |
| 18 | 02.86 | 38.80 | $22.009 \pm 0.012$ | $22.744 \pm 0.033$ | $25.040 \pm 0.349$ |
| 19 | 02.74 | 39.45 | $21.488 \pm 0.012$ | $21.955 \pm 0.022$ | $22.398 \pm 0.031$ |
| 10 | 04.59 | 19.52 | $25.078 \pm 0.075$ | $24.323 \pm 0.046$ | $24.935 \pm 0.036$ |
| 21 | 03.71 | 21.03 | $24.244 \pm 0.050$ | $24.843 \pm 0.099$ | $25.296 \pm 0.100$ |
| 22 | 03.10 | 24.52 | $21.192 \pm 0.012$ | $21.676 \pm 0.025$ | $22.144 \pm 0.035$ |
| 23 | 03.71 | 20.91 | $24.500 \pm 0.044$ | $24.867 \pm 0.073$ | $25.253 \pm 0.068$ |
| 24 | 01.36 | 34.39 | $22.841 \pm 0.022$ | $22.902 \pm 0.030$ | $23.370 \pm 0.044$ |
| 25 | 03.41 | 20.34 | $21.911 \pm 0.011$ | $22.184 \pm 0.015$ | $23.033 \pm 0.019$ |
| 26 | 04.56 | 12.53 | $23.703 \pm 0.033$ | $24.178 \pm 0.046$ | $24.744 \pm 0.035$ |
| 27 | 02.37 | 26.60 | $21.697 \pm 0.029$ | $21.899 \pm 0.038$ | $22.060 \pm 0.038$ |
| 28 | 04.34 | 12.89 | $23.309 \pm 0.030$ | $23.697 \pm 0.037$ | $24.336 \pm 0.031$ |
| 29 | 01.17 | 33.31 | $21.673 \pm 0.027$ | $21.583 \pm 0.029$ | $21.981 \pm 0.033$ |
| 20 | 02.76 | 20.96 | $21.347 \pm 0.009$ | $21.722 \pm 0.012$ | $22.284 \pm 0.013$ |
| 31 | 03.47 | 16.06 | $23.504 \pm 0.019$ | $23.813 \pm 0.029$ | $24.519 \pm 0.023$ |
| 32 | 02.75 | 20.84 | $21.357 \pm 0.009$ | $21.721 \pm 0.012$ | $22.282 \pm 0.012$ |
| 33 | 00.92 | 32.79 | $21.919 \pm 0.027$ | $21.762 \pm 0.023$ | $22.134 \pm 0.025$ |
| 34 | 02.79 | 17.85 | $22.655 \pm 0.020$ | $23.189 \pm 0.027$ | $23.575 \pm 0.022$ |
| 35 | 01.35 | 24.59 | $20.563 \pm 0.019$ | $20.852 \pm 0.020$ | $21.492 \pm 0.027$ |
| 36 | 01.83 | 19.54 | $20.163 \pm 0.005$ | $20.390 \pm 0.006$ | $20.966 \pm 0.006$ |
| 37 | 00.91 | 24.96 | $22.451 \pm 0.033$ | $23.143 \pm 0.052$ | $23.647 \pm 0.064$ |
| 38 | 01.92 | 16.63 | $22.821 \pm 0.021$ | $22.891 \pm 0.022$ | $23.381 \pm 0.017$ |

population, the age-metallicity degeneracy, the effects of internal extinction, possible variations in the initial mass function (IMF; e.g. Abraham et al. 1999), and the uncertainties in the absolute age zero point arising from these. Therefore, the use of spatially resolved colours has major advantages over that of the integrated colours alone.

We constructed CC diagrams and CMDs for both the Tadpole and the Mice galaxies on a pixel-by-pixel basis, following the recent studies by Abraham et al. (1999) and Eskridge et al. (2002) that showed the viability of such an approach. To avoid the spurious effects of noise in the sky background and to optimise the scientific return with respect to the processing time of the millions of pixel values, we only consider pixels with a minimum count level in the image with the lowest signal-to-noise (S/N) ratio. For the Tadpole system, this translated to a minimum count level of three times the sky noise in the F606W image, and for the Mice galaxies we used a $4\sigma_{\rm sky}$ level in the F475W image. The pixel CC diagrams, (F475W$-$F606W) vs. (F606W$-$F814W), and CMDs, F606W vs. (F606W $-$ F814W), of both galaxies are shown in Figs. 1, 2, 4 and 5. The data have been corrected for foreground extinction using the Schlegel et al. (1998) extinction map and the Galactic reddening law of Rieke & Lebofsky (1985): $A_{\rm F475W}/A_V \simeq 1.24$; $A_{\rm F606W}/A_V \simeq 0.90$; $A_{\rm F814W}/A_V \simeq 0.50$ mag. The arrows indicate the reddening and fading vectors for $A_V = 1.0$ mag (internal) extinction, assuming a foreground screen dust geometry.

### *3.2.1 Dissecting the Tadpole*

We have also included our cluster colour measurements in the CC diagrams of Figs. 1 and 4. Close inspection of the density distribution of pixels in the CC diagram of the Tadpole (Fig. 1) reveals a sharp drop in density to bluer colours below the dashed line. The lower-density plateau bluewards of this drop coincides approximately with the loci of the majority of the star clusters. Therefore, we define the region characterised by (F606W $-$ F814W) $\leq -0.7 \leq$ (F475W $-$ F606W) as Tadpole Region I of special interest. The pixels in this region also occupy a coherent region in colour-magnitude space, although not as sharply delineated as in colour-colour space (see Fig. 2). The slight density enhancement in Fig. 1 towards redder colours in (F475W $-$ F606W) and bluer colours in (F606W $-$ F814W) is an artificial feature caused by the lowest-S/N pixels in the F606W passband, located at the interface region between the galaxy and the sky background.

In the Tadpole CMD of Fig. 2, we define two further regions of interest. Region II consists of the pixels in the well-defined, bright, sharply delineated peak at F606W $\leq$ 26.8 mag; Region III is the fuzzy swarm of pixels on the redward side of that same peak. These three features occupy similar well-defined loci in all of the other CMDs that can be constructed from the available observations.

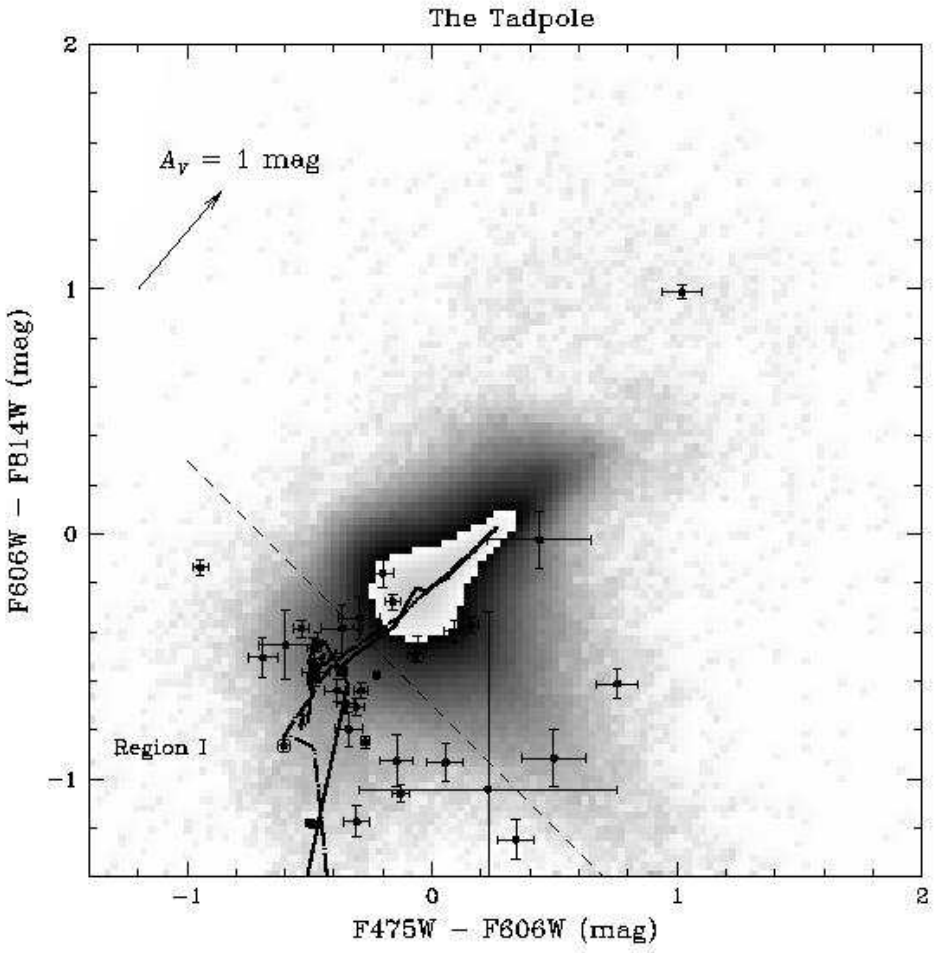


Fig. 1. Pixel CC diagram for the Tadpole galaxy. Region I is demarcated by the dashed line. The bullets with their associated error bars represent the cluster colours and their uncertainties; the thick solid and dash-dotted lines are the model predictions for the evolution of SSPs with solar metallicity ($Z = 0.020$) and $Z = 0.008$, respectively. The features in the models near (F475W − F606W) = −0.6 and (F606W − F814W) = −0.4 are caused by the appearance of red supergiants.

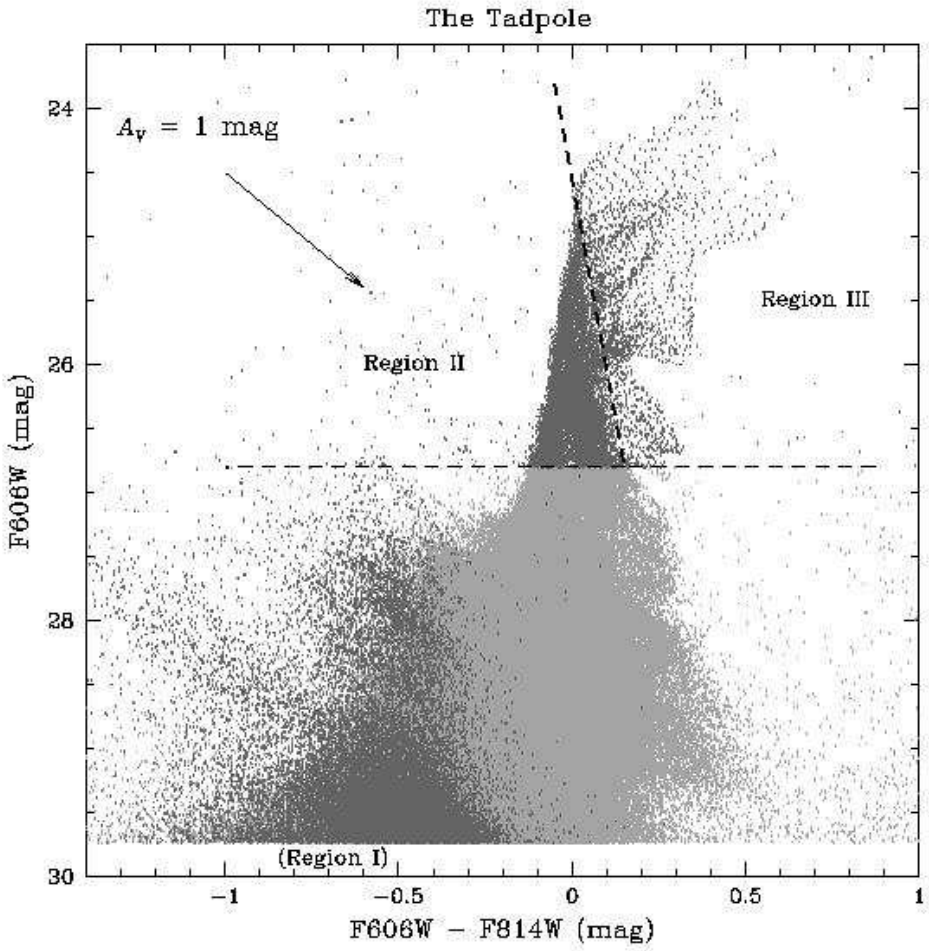


Fig. 2. Pixel CMD for the Tadpole galaxy. Specific features in the CMD are indicated by darker shading of the corresponding pixels and demarcated by dashed lines. The label "(Region I)" indicates the pixels corresponding to Region I defined on the basis of the CC diagram of Fig. 1.

In Fig. 3 we show the physical locations in the Tadpole system corresponding to these three features. The blue plateau in its CC diagram, Region I, corresponds to regions in which active star formation is currently taking place. A large fraction of the star clusters, indicated by circles, appears to be as-

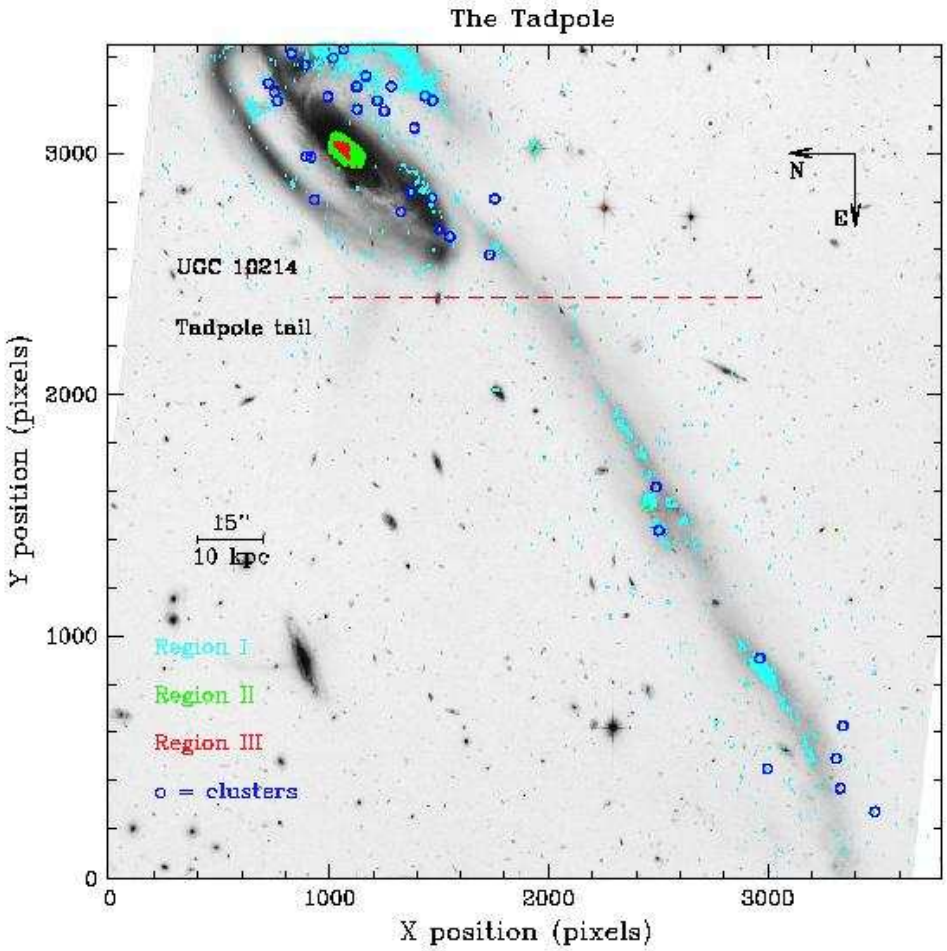


Fig. 3. Representation of the Tadpole galaxy on a pixel-by-pixel basis overlaid on a grey-scale rendition of the true-colour press release image. The specific features identified from the CC diagram of Fig. 1 and the CMD of Fig. 2 are colour coded; the areas adopted for our comparison of the physical properties of the main galactic disk and the tidal tail are separated by the horizontal dashed line.

sociated with these areas as well. The sharply delineated bright peak in the Tadpole CMD corresponds to the core of the dominant spiral galaxy UGC 10214, a projected area occupying roughly $3.1 \times 1.2$ kpc along the galaxy's major axis, while the bright fuzzy swarm of red pixels is located in the galactic disk underlying the sharp bright peak in the centre region of $\sim 6.2 \times 3.1$ kpc, elongated along the galaxy's major axis and not corrected for the galaxy's inclination. Although these latter pixels have redder colours than those in the galactic centre, a close inspection of the individual observations and of the "true-colour" image of Ford et al. (2002) does not reveal significant amounts of extinction surrounding the immediate centre of the galaxy; these pixels are not associated with the dust lane seen at slightly larger radii. Thus, we conclude that the central galactic disk stellar population is intrinsically redder than the population in its very core. This may indicate stronger present or more recent star formation in the core (see e.g. NGC 7252; Whitmore et al. 1993), or perhaps low-level nuclear (Seyfert or LINER) activity, such as seen in a number of early-type spiral galaxies with blue cores (e.g. Windhorst et al. 2002). Near-infrared photometry in an $8''$ aperture centred on the galactic centre (Joseph et al. 1984) classifies the galactic centre as relatively "normal", without the $(K - L)$ excess expected from a recent burst of star formation.

Finally, we compared the distributions and densities in colour-colour and colour-magnitude space of the pixels originating in the tidal tail and the galactic disk itself (see Fig. 3). While the colours of the tidal tail and of the main galactic disk occupy very similar areas in the CC diagram, the pixels in the tidal tail are *dominated* by "Region I" colours: $\sim 60\%$ of the pixels in the tidal tail correspond to colours in Region I. They contribute $\sim 70, 55$, and 40% of the total flux in the F475W, F606W, and F814W passbands, respectively. (Only a small fraction of the light from the main disk of the galaxy corresponds to "Region I"-type colours.) The colours of the remaining pixels coincide with the colours of the main galactic disk.

### *3.2.2 Unraveling the Mice*

Although the drop in density towards bluer colours in the CC diagram of the Mice (see Fig. 4) is not as sharp as for the Tadpole, we see that the star clusters are predominantly found in the same region in colour-colour space as before. Therefore, we adopt the same definition as for the Tadpole for Region I in the Mice. The difference between the Mice and the Tadpole in the sense that we observe a more gradual decrease in density towards bluer colours in the Mice than in the Tadpole indicates most likely a real difference in the SFH of both systems. In the Tadpole, the interaction has affected only small regions of the system because of the relatively minor gravitational disturbance of the lower-mass galaxy on the higher-mass one (see Section 4.2), while the active star formation is more widespread throughout both galaxies and the

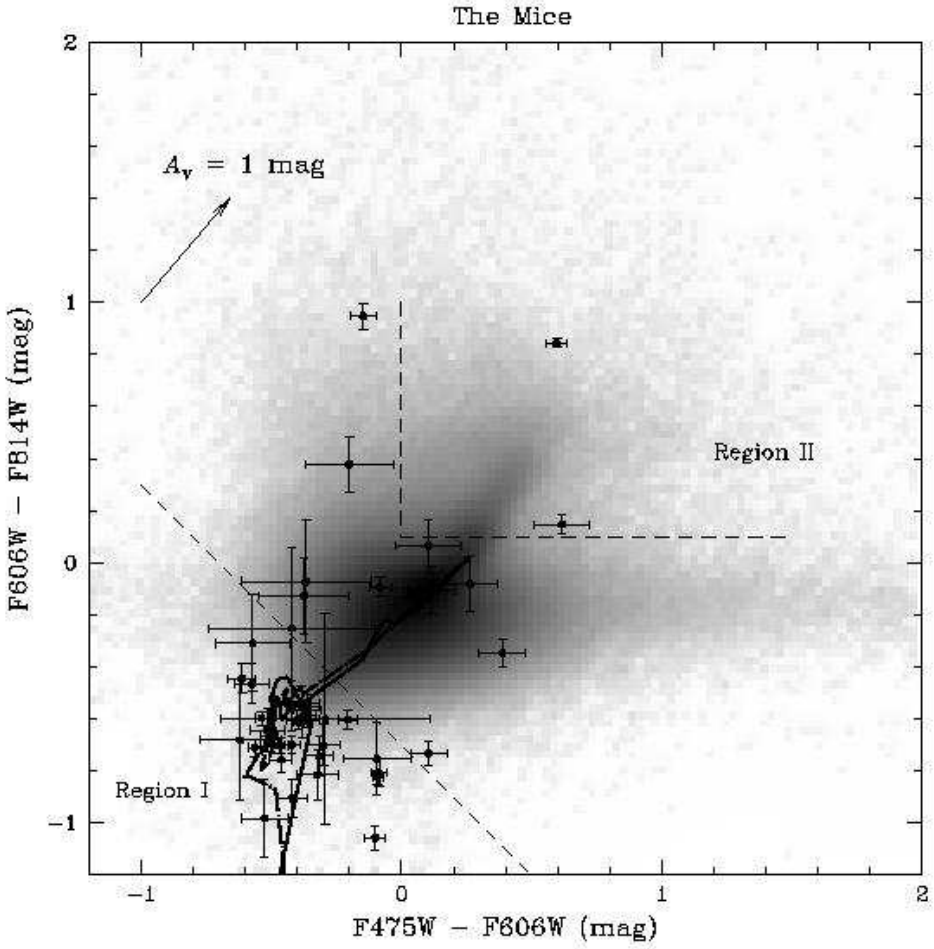


Fig. 4. Pixel CC diagram for the Mice. Figure coding is as in Fig. 1.

tidal tails of the Mice.

The Mice CC diagram shows a red extension, roughly characterised by (F475W−F606W) $\geq$ 0.0 mag and (F606W − F814W) $\geq$ 0.2 mag. Further verification of this feature in the CMD (Fig. 5) shows that we also need to restrict the pixels in this feature, Region II, to obey F606W $\leq$ 28.0 mag, to avoid contamination by low-S/N pixels and background noise.

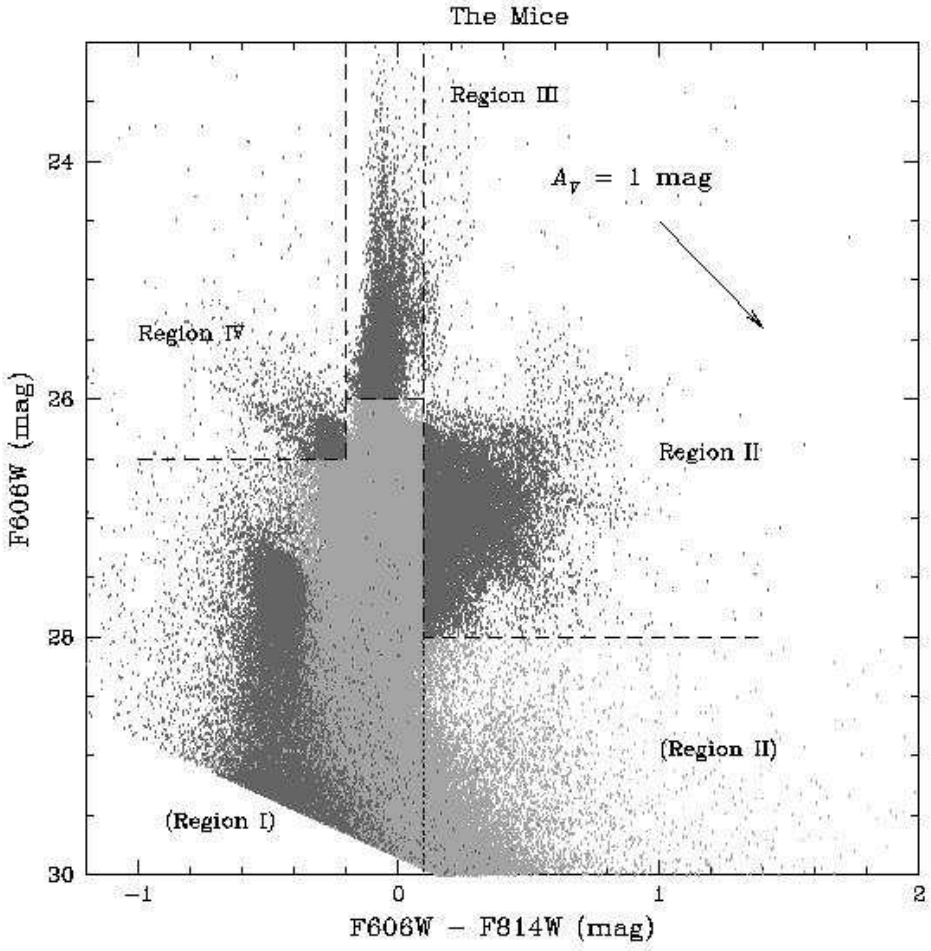


Fig. 5. Pixel CMD for the Mice. Figure coding is as in Fig. 2. The definition of Region II based on the CC diagram of Fig. 4 includes all pixels redder than the vertical demarcation at (F606W − F814W) = 0.1; based on this CMD, however, we further restricted this region to pixels brighter than F606W = 28 mag.

The "plume" of enhanced density in Fig. 4 at (F606W − F814W) $\sim -0.2$ mag is an artificial feature caused by the lowest-S/N pixels in the F475W passband.

We define two further regions of interest in the Mice: Region III consists of

the bright peak with pixel values brighter than F606W = 26.0 mag, while it appears that a further plume in the CMD, starting at the faint limit of the bright peak, but with bluer colours, might be a physically distinct population of pixels. We define Region IV to be composed of pixels with F606W $\leq$ 26.5 mag, and (F606W $-$ F814W) $\leq -0.2$ mag. Again, all of these features occupy similarly well-defined loci in the other CMDs that can be constructed from the available observations.

In Fig. 6, we show the correspondence between the features in the CC diagram and the CMDs of the Mice and their physical locations in the system itself. Again, we see that all of the features we identified coincide with physically distinct regions in the galaxies. Region I again coincides with regions of active star formation, and a fairly good match with the locations of the star clusters is observed once more. Region II is associated with areas of heavy extinction.

Although we did not define a similar region as Region II in the CC diagram of the Tadpole galaxy, this is merely due to the sharper demarcation of Region II in the Mice, and not to the absence nor even the lower density of such red pixels in the Tadpole system. The sharper demarcation in the Mice indicates that the dust and stellar populations are less well mixed in this system than in the Tadpole (or that dust is more important in the Mice). We attribute this to the difference in viewing angle between the two systems. The dust lanes are most clearly seen and most sharply defined in the edge-on view of NGC 4676A, while the dust is seen through an upper layer of stars in the Tadpole galaxy, which hence appears to be better mixed in projection.

The bright peak of Region III is clearly identified as the population of pixels originating from the centre of the southern galaxy, NGC 4676B. The width of the bright peak in the CMD of the Mice is smaller than that in the Tadpole CMD. It therefore appears that the contrast between the blue core and the redder central region in the Tadpole is of real significance.

The slightly fainter but bluer feature of Region IV is associated with central star forming regions in both galaxies in the system. Both NGC 4676A and NGC 4676B are located in the region occupied by the "normal" galaxies in the near-infrared $(K-L)$ vs. $(H-K)$ diagram of Joseph et al. (1984), without the $(K-L)$ excess indicative of recent nuclear star formation. This is confirmed by the relatively inconspicuous and red CMD features associated with the galactic centres, and the low far-infrared luminosity of the system (Hibbard 1995, Hibbard & van Gorkom 1996).

A comparison between the CMDs and CC diagrams of the individual galaxies of the Mice does not reveal significant differences that cannot be explained by the different viewing angles. For instance, Region II is not as densely populated in the CC diagram of NGC 4676B as in that of NGC 4676A, but this is

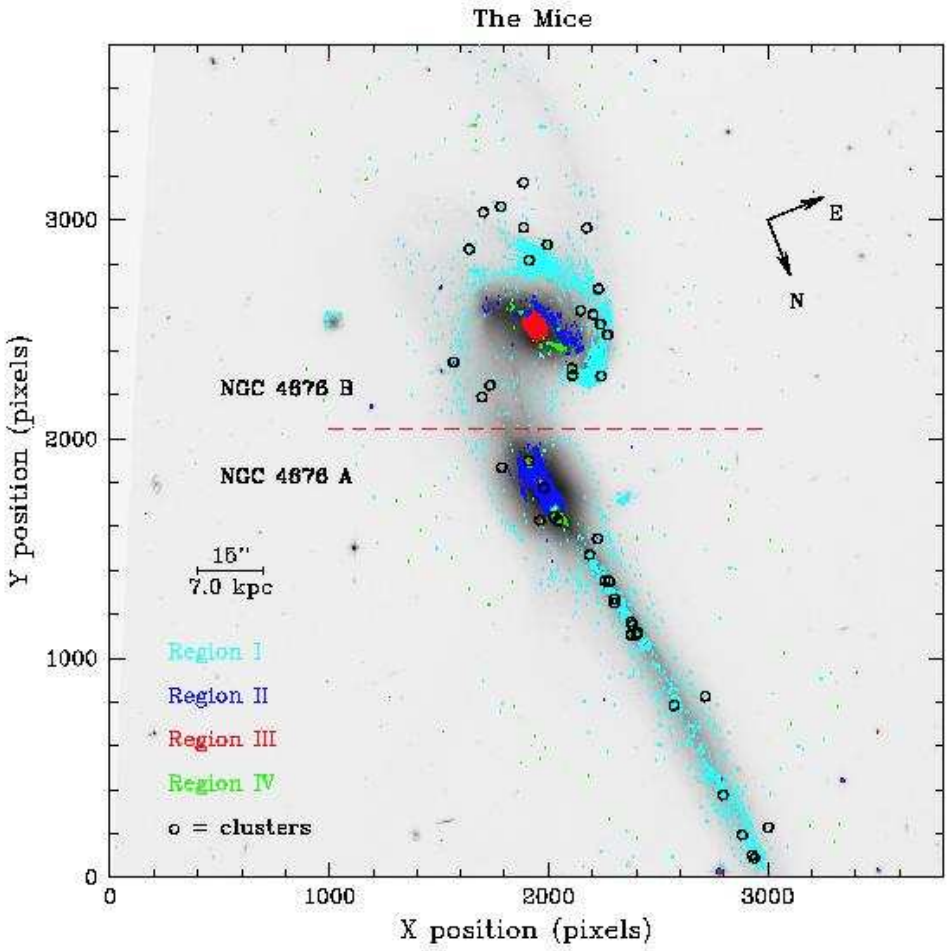


Fig. 6. Representation of the Mice system on a pixel-by-pixel basis. The specific features identified from the CC diagram of Fig. 4 and the CMD of Fig. 5 are colour coded, and overlaid on a grey-scale rendition of the true-colour press release image; the areas adopted for our comparison of the physical properties of both galaxies are separated by the horizontal dashed line.

likely due to the more face-on orientation of the former galaxy. Region I is approximately similarly well populated in both CC diagrams; $\sim (1.5 - 2.5)\%$ of the total number of pixels with F475W fluxes in excess of the $4\sigma_{\rm sky}$ level are found in Region I. This indicates that the burst of star formation triggered by the encounter is similar in both galaxies and has affected only relatively small areas in either galaxy, in particular in their tidal tails and outer spiral arms.

## 4 Implications for star and cluster formation scenarios

### *4.1 Dynamical time-scales and cluster formation in the Mice*

Starting with Toomre & Toomre (1972)'s seminal paper based on a small number of test particles, sophisticated *N*-body simulations have been employed to generate an interaction morphology resembling that observed for the Mice (e.g. Mihos et al. 1993, Gilbert & Sellwood 1993, Barnes 1996, Sotnikova & Reshetnikov 1998). The current state of the art simulations seem to converge to agreement on the interaction geometry, inclination angles of the individual galaxies, parabolic orbital parameters, and a mass ratio of the two galaxies of roughly unity (e.g. Barnes 1996, Sotnikova & Reshetnikov 1998) to 1:2 for NGC 4676A : NGC 4676B (Hibbard 1995, Hibbard & van Gorkom 1996) [from HI rotation curves]. While the morphological features are fairly well reproduced in most respects, matching the kinematic properties of the entire system including the tidal tails requires the presence of extended massive dark matter haloes surrounding both galaxies (Sotnikova & Reshetnikov 1998), but see Gilbert & Sellwood (1993) for an opposing view.

The system's morphology suggests that the Mice represents a galaxy merger in its very early stages (e.g. Toomre 1977); current best estimates for the time-scale since pericentre are $\sim (160 - 180) \times 10^6$ yr (Mihos et al. 1993, Barnes 1996). In order to facilitate a comparison of the relevant time-scales, in Figs. 1 and 4 we have overplotted the model predictions for the evolution of SSPs, based on the SSP models of Schulz et al. (2002), properly folded through the *HST*/ACS filter response curves and taken account of the better-than-expected in-flight performance (Gilliland, priv. comm.). We added the age-dependent contributions of an exhaustive set of gaseous emission lines and of gas continuum emission to the Schulz et al. (2002) models. Emission-line contributions to optical broad-band fluxes are very important during the first $\simeq 3 \times 10^7$ yr of evolution for subsolar metallicities ($Z = 0.004 = 0.2 Z_\odot$). For solar metallicity SSPs, their contribution is slightly lower but still important for $t \lesssim 1.2 \times 10^7$ yr (Anders et al. 2002). We assume roughly solar metallicity for the star clusters: for star formation associated with any reasonable interaction scenario in the present-day Universe one can expect metallicities in the range

$(0.5 - 1.0) Z_{\odot}$ (Fritze–v. Alvensleben & Gerhard 1994).

Due to the almost parallel age and extinction vectors, we cannot determine the ages of the star clusters unambiguously, nor correct their magnitude measurements for the effects of extinction. However, Fig. 4 shows that the majority of the bright clusters in the Mice are located in Region I, with only a small spread along the extinction and age vectors. The other, redder clusters could be either part of an older cluster population, or more heavily affected by extinction. If we assume that for the blue clusters in Region I the combination of foreground and internal extinction is small or negligible, this allows us to place a lower limit on their age. However, such a lower limit is highly uncertain due to two further complications: *(i)* the majority of the bluest star clusters are located in the region of the CC diagram where the models are multi-valued; and *(ii)* the resulting age estimates are a strong function of metallicity for such young ages, even for a close-to-solar metallicity range. Nevertheless, the available data for the Mice imply a minimum age for the majority of the blue clusters of $(1.0 \pm 0.2) \times 10^8$ yr for solar metallicity, or $t_{\rm min} \sim 2 \times 10^8$ yr for $Z = 0.4\, Z_{\odot}$. (Note that because of the good match of our models to the observed colours we can recover all of parameter space by mixing various amounts of young and old[er] stellar populations with extinction. This implies that our basic assumption that we can use pixel CMDs and CC diagrams as composites of SSPs is a reasonable approximation to reality.)

We are now in a good position to comment on the importance of star cluster formation in the context of the tidally-induced violent star formation in the general field population. A large fraction of the bluest clusters coincide spatially with the blue field population in the spine of the NGC 4676A tidal tail and the outer spiral arm of NGC 4676B (see Fig. 6). H$\alpha$ observations of the Mice (Stockton 1974, Mihos et al. 1993, Hibbard 1995, Hibbard & van Gorkom 1996, Sotnikova & Reshetnikov 1998), indicative of recent star formation, are consistent with a tidal origin. A detailed comparison of Fig. 6 with the H$\alpha$ map in Hibbard (1995) shows remarkably good agreement between the H$\alpha$-bright condensations and features within the tidal tails and the outer spiral arms of NGC 4676B, and the spatial distribution of the bluest pixels (Regions I and IV) in the Mice (Figs. 4 and 5).

We can, in fact, place a strong lower limit on the age of the H$\alpha$-bright regions in the Mice. Stockton (1974) concluded, from his H$\alpha$+[NII] spectroscopy, that all of the emission from NGC 4676A, including the entire length of the tidal tail, and from at least part of NGC 4676B is A-star dominated. The most likely origin for such an A-type spectrum is rapid, widespread star formation that effectively ceased $\gtrsim 5 \times 10^7$ yr ago, so that earlier-type O and B stars would have had sufficient time to evolve off the main sequence. This is consistent with the *current* star formation rates derived by Sotnikova & Reshetnikov (1998) in both NGC 4676A and its tidal tail, which are not unlike the rates

found in normal spiral galaxies. This implies, therefore, that these parts of the interacting system are currently not undergoing enhanced star formation due to the encounter, but did so $> 5 \times 10^7$ yr ago.

Secondly, Elmegreen et al. (1993) and Sotnikova & Reshetnikov (1998) suggest that the actual mechanism responsible for the star formation in the H$\alpha$ condensations is driven by gravitational instabilities in the gas caused by the encounter. They calculate that the time-scale for developing such instabilities is on the order of a few times $10^7$ yr, which places a similar lower limit on the age of these compact objects. Therefore, the main event triggering the cluster formation must have occurred at least $\sim (1.5 - 2.0) \times 10^8$ yr ago, depending on the precise cluster metallicities.

We conclude, therefore, that Regions I and IV in the CC diagram of the Mice correspond to active and recent star formation induced by the tidal interaction, while the star clusters found scattered throughout these star-forming regions are *also* consistent with having been formed on similar time-scales.

The fractional contribution of the star clusters to the total flux in Region I in the Mice is $\sim 40\%$, independent of wavelength. Because of our selection bias towards brighter star clusters, this is in fact a lower limit to the total cluster contribution. Despite the fact that this region is not as sharply defined in the Mice as in the Tadpole system, this clearly shows that star cluster formation is a major mode of star formation in galactic encounters.

Some 40% of the star cluster candidates identified in Section 3.1 coincide spatially (in projection) with the H$\alpha$-bright condensations, which therefore might be either young star clusters, knots of active star formation, giant HII complexes (Hibbard 1995, Hibbard & van Gorkom 1996, Sotnikova & Reshetnikov 1998), or due to projection effects. Most of the objects are unresolved by the ACS PSF, and therefore have diameters of $\lesssim 35$ pc.

If we assume that the ongoing tidal interactions between NGC 4676A and NGC 4676B have indeed induced the formation of the observed bright blue star clusters in the past $\sim 2 \times 10^8$ yr, we can estimate the cluster masses and compare those to the masses of star clusters in other young cluster systems. The bright blue star clusters in the Mice exhibit a peak in their brightness distribution at F606W $\sim$ 22 mag; combined with the mass-to-light ($M/L$) ratio in the F606W passband at an age of $\lesssim 2 \times 10^8$ yr, $M/L_{606} \lesssim 0.2$, we estimate a characteristic photometric mass for these clusters of $\lesssim 3 \times 10^6 M_\odot$.

We emphasize that we are only sampling the bright wing of the CLF, and therefore the high-mass wing of the cluster mass function. Independent dynamical mass estimates are available only for a few of the most luminous SSCs, and are approximately $10^6 M_\odot$ (Ho & Filippenko 1996a, Ho & Filippenko 1996b, Smith & Gallagher 2001). The masses of Galactic globular clusters are

typically in the range $10^4 - 3 \times 10^6 M_\odot$ (e.g. Mandushev et al. 1991, Pryor & Meylan 1993). Thus, the approximate photometric mass estimate obtained for the median of the bright blue clusters in the Mice is consistent with this being the bright wing of a "normal" SSC or globular cluster progenitor population.

### *4.2 Star and cluster formation in the Tadpole galaxy*

The Tadpole system is an example of a galaxy encounter between two unequal-mass galaxies at a later stage. The system is composed of a mildly disturbed SBc galaxy and a long, low-S/N tidal tail. The latter shows a number of bright, blue condensations, while active star formation is also apparent on the inside of the western spiral arm (Fig. 3). Ford et al. (2002) attribute this region of enhanced star formation to the remnant of a low-mass galaxy that caused the disturbed appearance of the system.

As for the Mice, in Fig. 1 we have overplotted the model predictions for the evolution of SSPs. We see that the majority of the star clusters are located in a very similar region as the clusters in the Mice, again with a relatively small spread along the age/extinction vector. In view of the formation constraints imposed by the time-scale to develop gravitational instabilities, we conclude that the clusters we identified in the Tadpole (Table 2) must also have been formed very recently, $\sim (1.5 - 2.0) \times 10^8$ yr ago, and represent the high-mass wing of a similar mass distribution as in the Mice. This minimum age estimate is consistent with their spatial distribution throughout the galactic disk and tidal tail, which matches the actively star forming regions defined by the pixels in Region I reasonably well. The clusters located in Region I of the Tadpole CMD contribute $\gtrsim 35\%$ to the total flux of all pixels in this region, again independent of passband for the filter combination used here.

It is rather remarkable that the interaction of a massive SBc galaxy and a low-mass companion caused such a strong deformation of the massive galaxy and also very pronounced star *cluster* formation. We can obtain a rough, independent estimate of the dynamical age of the interaction in the Tadpole interacting system by comparing the length of its tail ($\sim 110$ kpc) to the stellar velocity dispersion expected in the undisturbed progenitor galaxy. In a typical large spiral galaxy, velocity dispersions of $\sim (150 - 300)$ km s$^{-1}$ are expected (Tremaine et al. 2002), so that the dynamical age since the beginning of the interaction resulting from this impulse approximation is $t_{\rm dyn} \sim (4 - 8) \times 10^8$ yr. This is remarkably close to the ages of the star clusters estimated from their loci in the CC diagram.

## 5 Summary and Conclusions

We have utilised optical pixel-by-pixel CMDs and CC diagrams to explore and deduce the star and star cluster formation histories of the Mice and the Tadpole interacting galaxies. Despite their considerable distance of $\gtrsim 100$ Mpc, this technique now offers promising prospects to study the local, dominant stellar populations out to greater distances than ever before thanks to the capabilities of the Advanced Camera for Surveys onboard *HST*. The analysis performed in this paper is based on a subset of the ACS Early Release Observations, obtained from the *HST* data archive. One of the main advantages of ACS/WFC observations is that the PSF is (marginally) undersampled, so that each pixel corresponds to a spatially independent measurement of the underlying composite stellar population.

In both interacting systems we find some 40 bright young star clusters ($20 \lesssim$ F606W(mag) $\lesssim 25$, with diameters $\lesssim 35$ pc and a characteristic mass of $\sim 3 \times 10^6 M_\odot$), which are spatially coincident with blue regions of active star formation in the tidal tails and spiral arms of our target galaxies. Despite the complications caused by the age–extinction degeneracy in the combination of the F475W, F606W and F814W optical passbands, we estimate that the main event triggering the formation of these clusters occurred $\sim (1.5 - 2.0) \times 10^8$ yr ago. It is therefore likely that the gravitational interactions responsible for the disturbed appearances of our target galaxies have induced not only enhanced star formation, but also star cluster formation. We argue that star cluster formation is a major mode of star formation in galactic interactions, with $\gtrsim 35\%$ of the active star formation in encounters occurring in star clusters. This is the first time that young star clusters have been detected along the tidal tails in interacting galaxies.

We find that specific features and plumes in the CMDs and CC diagrams of both interacting systems correspond to sharply demarcated regions in the systems themselves. In the Tadpole system, we detect a hitherto unknown very bright blue core superimposed on a redder central area, which we speculate may be related to some form of nuclear activity in the main disk galaxy of this system, UGC 10214. The tidal tail of the system is dominated by blue star forming regions, which occupy some 60% of the total area covered by the tail; they contribute $\sim 70\%$ of the total flux in the F475W passband (decreasing to $\sim 40\%$ in F814W). The remaining pixels in the tail have colours consistent with those of the main disk.

The Mice interacting galaxies are an example of an approximately equal-mass encounter. We identify regions of pronounced star formation in the tidal tails, outer spiral arms, and near the galactic centres. We conclude that the tidally triggered burst of star formation is of similar strength in both galaxies, but it

has affected only relatively small spatially coherent areas.

Finally, the analysis in this paper has shown that the technique of using both CMDs and CC diagrams on a pixel-by-pixel basis, combined with measurements of individual, distinct compact objects, is a very powerful tool to unravel the complex star formation histories and their associated star cluster formation in interacting galaxies.

## Acknowledgements

JTL and MCMH acknowledge PPARC funding to attend the 2002 PPARC/ Cambridge International Undergraduate Summer School. We thank Paul Eskridge, Max Mutchler, Ronald Gilliland, Rolf Jansen, and Richard Sword for scientific or graphics suggestions and support. This research has made use of NASA's Astrophysics Data System Abstract Service. The Interactive Data Language (IDL) is licensed by Research Systems Inc., of Boulder, CO, USA.

## References

Abraham, R.G., Ellis, R.S. Fabian, A.C., Tanvir, N.R., Glazebrook, K., 1999, MNRAS, 303, 641-658.

Anders, P., Fritze–v. Alvensleben, U., de Grijs, R., 2002, MNRAS, in prep.

Balcells, M., Peletier, R.F., 1994, AJ, 107, 135-152.

Barnes, J.E., 1996, in: Kennicutt, R.C., Schweizer, F., Barnes, J.E. (eds) Galaxies: Interaction and Induced Star Formation, Lecture Notes of the SAAS-FEE Advanced Course 26, SSAA, Springer: Berlin, p. 320-323.

Bothun, G.D., 1986, AJ, 91, 507-516.

Buzzoni, A., 1997, in: Sato, K. (ed) IAU Symp. 183, Cosmological Parameters and the Evolution of the Universe, Boston: Kluwer, p. 134-139.

de Grijs, R., Bastian, N., Lamers, H.J.G.L.M., 2002a, MNRAS, submitted

de Jong, R.S., 1996, AA, 313, 377-395.

Elmegreen, B.G., Kaufman, M., Thomasson, M., 1993, ApJ, 412, 90-98.

Eskridge, P.B., Taylor, V.A., Windhorst, R.A., Odewahn, S.C., Chiarenza, C.A.T., Conselice, C.J., de Grijs, R., Frogel, J.A., Matthews, L.D., O'Connell, R.W., Gallagher, J.S., 2002, ApJ, submitted

Ford, H., Illingworth, G., Clampin, M., et al., 2002, NASA press release, STScI-PR02-11, 30 April 2002 (http://oposite.stsci.edu/pubinfo/pr/2002/11/)

Franceschini, A., Silva, L., Fasano, G., Granato, G.L., Bressan, A., Arnouts, S., Danese, L., 1998, ApJ, 506, 600-620.

Fritze–v. Alvensleben, U., Gerhard, O.E., 1994, AA, 285, 751-774.

Gilbert, S.J., Sellwood, J.A., 1993, in: Franco, J., Lizano, S., Aguilar, L., Daltabuit, E. (eds) Numerical Simulations in Astrophysics, Cambridge Univ. Press, Cambridge, p. 131-134.

Hibbard, J.E., 1995, Ph.D. Thesis, Columbia University

Hibbard, J.E., van Gorkom, J.H., 1996, AJ, 111, 655-695.

Ho, L.C., Filippenko, A.V., 1996a, ApJ, 466, L83-L86

Ho, L.C., Filippenko, A.V., 1996b, ApJ, 472, 600-610.

Joseph, R.D., Meikle, W.P.S., Robertson, N.A., Wright, G.S., 1984, MNRAS, 209, 111-122.

Kong, X., Zhou, X., Chen, J., et al., 2000, AJ, 119, 2745-2756.

Krist, J., Hook, R., 2001, The Tiny Tim User's Guide, Version 6.0 (http://www.stsci.edu/software/tinytim/)

Mandushev, G., Staneva, A., Spasova, N., 1991, AA, 252, 94-99.

Mihos, J.C., Bothun, G.D., Richstone, D.O., 1993, ApJ, 418, 82-99.

Pavlovsky, C., et al., 2001, ACS Instrument Handbook, Version 2.1, STScI, Baltimore (http://www.stsci.edu/hst/acs/documents/handbooks/cycle11/cover.html)

Peletier, R.F., Balcells, M., 1996, AJ, 111, 2238-2242.

Peletier, R.F., Balcells, M., Davies, R.L., Andredakis, Y., Vazdekis, A., Burkert, A., Prada, F., 1999, MNRAS, 310, 703-716.

Pryor, C., Meylan, G., 1993, in: Djorgovski, S.G., Meylan, G. (eds) Structure and Dynamics of Globular Clusters, A.S.P.: San Francisco, p. 357-371.

Rieke, G.H., Lebofsky, M.J., 1985, ApJ, 288, 618-621.

Schlegel, D.J., Finkbeiner, D.P., Davis, M., 1998, ApJ, 500, 525-553.

Schulz, J., Fritze–v. Alvensleben, U., Möller, C.S., Fricke, K.J., 2002, AA, 392, 1-11

Smith, L.J., Gallagher, J.S., 2001, MNRAS, 326, 1027-1040.

Sotnikova, N.Ya., Reshetnikov, V.P., 1998, AstL, 24, 73-83.

Stetson, P.B., 1987, PASP, 99, 191-222.

Stockton, A., 1974, ApJ, 187, 219-221.

Terndrup, D.M., Davies, R.L., Frogel, J.A., DePoy, D.L., Wells, L.A., 1994, ApJ, 432, 518-546.

Toomre, A., 1977, in: Tinsley, B.M., Larson, R.B. (eds) The Evolution of Galaxies and Stellar Populations, Yale Univ. Press: New Haven, p. 401-426.

Toomre, A., Toomre, J., 1972, ApJ, 178, 623-666.

Tremaine, S., Gebhardt, K., Bender, R., et al., 2002, ApJ, 574, 740-753.

Vorontsov-Vel'yaminov, B.A., 1958, Astr. Zh., 35, 858 (English transl. in Soviet Astr., 2, 805-813.)

Whitmore, B.C., Schweizer F., Leitherer, C., Borne, K., Robert, C., 1993, AJ, 106, 1354-1370, 1702-1706.

Windhorst, R.A., Taylor, V.A., Jansen, R.A., et al., 2002, ApJS, 143, in press (November issue; `http://www.arXiv.org/astro-ph/0204398`)